ACS APPLIED MATERIALS & INTERFACES

www.acsami.org

Research Article

Stable Li–Metal Batteries Enabled by in Situ Gelation of an Electrolyte and In-Built Fluorinated Solid Electrolyte Interface

Xiaoxia Jiao, Jin Wang, Guixia Gao, Xuezhi Zhang, Cuimei Fu, Lina Wang,* Yonggang Wang,* and Tianxi Liu

Cite This: *ACS Appl. Mater. Interfaces* 2021, 13, 60054–60062

Read Online

ACCESS | Metrics & More | Article Recommendations | Supporting Information

ABSTRACT: Lithium–metal batteries (LMBs) are the focus of upcoming energy storage systems with extremely high-energy density. However, the leakage of liquid electrolyte and the uncontrollable dendritic Li growth on the surface of the Li anode lead to their low reversibility and safety risks. Herein, we propose a stable quasi-solid LMB with in situ gelation of liquid electrolyte and an in-built fluorinated solid electrolyte interface (SEI) on the Li anode. The gel polymer electrolyte (GPE) is readily constructed via cationic polymerization between lithium hexafluorophosphate and ether electrolyte. The fluorine-containing additive, fluoroethylene carbonate (FEC), plays a crucial role in the building of a dense SEI with fast interfacial charge transport. The ex situ spectroscopic characterizations suggest that the enhanced LiF species in the SEI with the addition of FEC and the in situ optical microscopy reveal the inhibited dendritic Li growth. Moreover, GPE@FEC exhibits a high oxidative stability beyond 5.0 V (vs Li/Li$^+$). The significantly improved Li plating/stripping efficiency (400 cycles, 98.7%) is presented for the Li||Cu cells equipped with GPE@FEC. Decent cycling stability is also available for the cells with the $LiFePO_4$ cathode, reflecting the feasibility of GPE@FEC for practical LMBs with enhanced stability and safety.

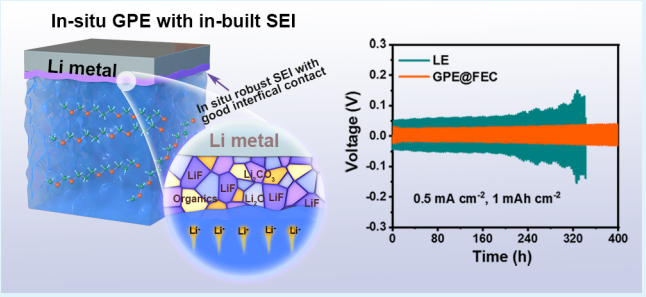

KEYWORDS: *lithium–metal battery, in situ gelation, gel polymer electrolyte, solid electrolyte interface, lithium dendrites*

Downloaded via DONGHUA UNIV LIB on March 7, 2022 at 04:45:47 (UTC).
See https://pubs.acs.org/sharingguidelines for options on how to legitimately share published articles.

1. INTRODUCTION

Electric vehicles with long driving range have stimulated the development of high-energy density storage devices.[1,2] The insufficient capacity of graphite-based anodes has limited the ability for lithium–ion batteries (LIBs) to meet the modern needs of electric vehicles.[3−5] The low reduction potential (−3.04 V vs SHE) as well as ultrahigh theoretical specific capacity (3860 mAh g^{-1}) have raised hopes for metallic Li to be the anode of the new generation of lithium–metal batteries (LMBs).[6,7] Despite the outstanding advantages, Li anodes suffer from continuous corrosion and uncontrolled dendritic Li growth at the electrode/electrolyte interface when in contact with organic liquid electrolytes (LEs). Battery failure and internal short circuits may occur upon a repeated Li plating/stripping process.[8−10]

At present, gel polymer electrolytes (GPEs) and solid-state electrolytes (SSEs) have shown improved stabilities toward Li anodes over traditional LEs for prospective LMBs.[11−21] Nevertheless, GPEs and SSEs have usually been prepared in self-standing films before being integrated into cells. The bottom part of the cathode hardly touches the electrolyte film, leading to incomplete capacity release. To overcome the contact problems, interphase design strategies have been proposed, among which the approach to create a polymer framework via an in situ gelation process within cells has been shown to be very desirable.[22−27] The liquid phase that does not participate in polymerization is entrapped by the in situ generated polymer framework, enabling high bulk ionic conductivity. Therefore, the cathode structure is fully filled with the GPEs, leading to good wettability.

Despite that the interfacial charge transport in the cathode has been promoted, the in situ GPEs do not guarantee that the reversible electrochemistry of the Li–metal anode will be sustained. Previously, it has been believed that the quasi-solid/solid-state GPEs/SSEs with a high mechanical modulus would physically suppress the Li dendrites.[28,29] Indeed, the recent studies have overturned the old views and revealed the possible penetration of Li dendrites into SSEs.[30−32] The security risks and large volume change owing to the inhomogeneous Li deposition still remain big challenges. An autogenetic solid–electrolyte interface (SEI) on the Li anode with high chemical stability, mechanical strength, and ionic conductivity would conquer the limitations. Various electrolyte additives including

Received: October 15, 2021
Accepted: November 29, 2021
Published: December 9, 2021

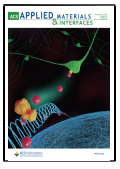

© 2021 American Chemical Society

https://doi.org/10.1021/acsami.1c19663
ACS Appl. Mater. Interfaces 2021, 13, 60054–60062

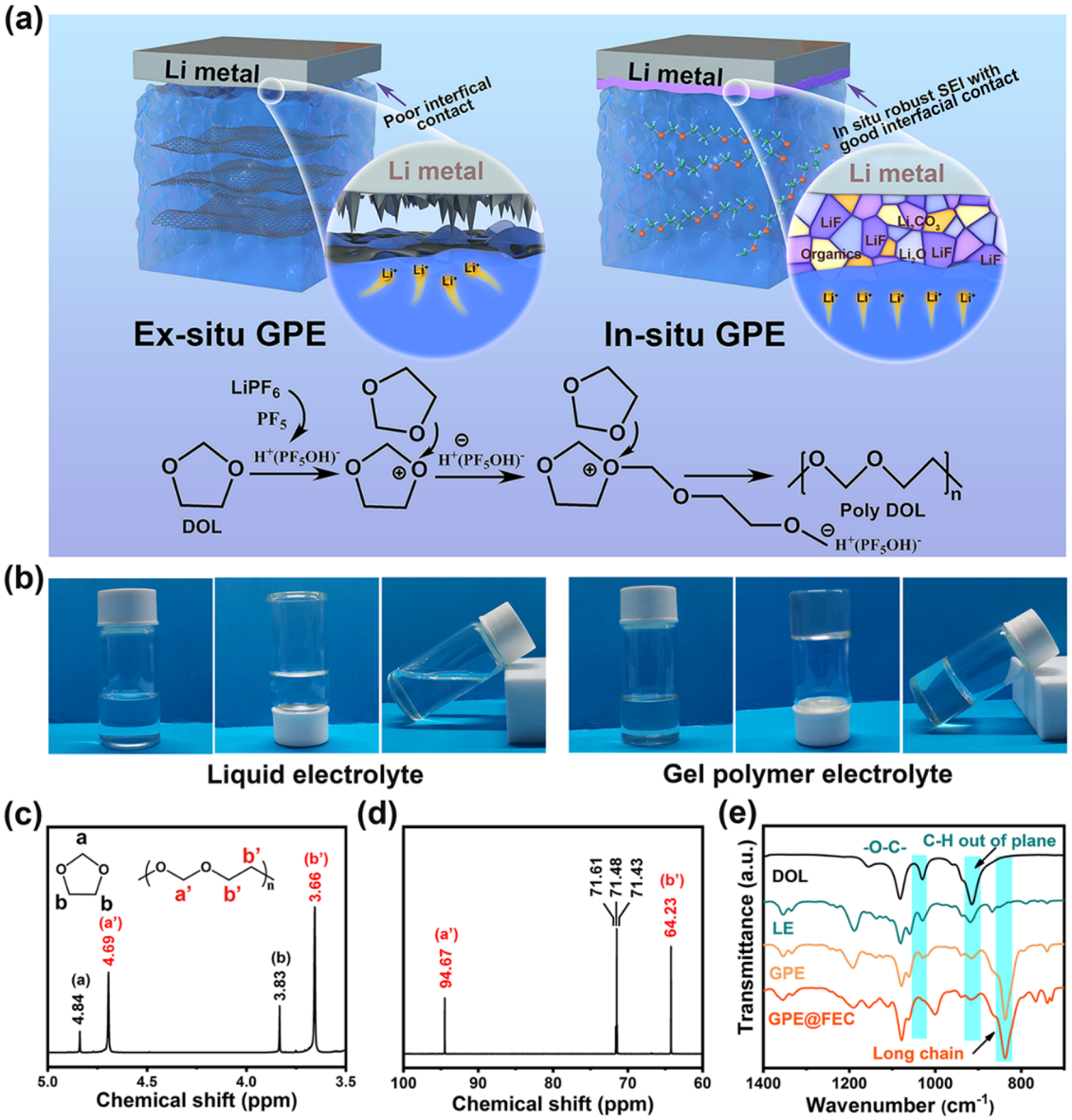

Figure 1. Preparation and spectroscopic characterizations of in situ GPE. (a) Schematic illustration of the interfacial contact between the Li−metal anode and ex situ GPE or in situ GPE. Inset: The reaction mechanism of the polymerization of DOL. (b) Optical photographs of LE and GPE@FEC. (c) ^{1}H NMR and (d) ^{13}C NMR spectra of GPE@FEC. (e) FTIR spectra of DOL, LE, GPE and GPE@FEC.

fluoroethylene carbonate (FEC),[33−36] vinylene carbonate (VC),[37] lithium chloride,[38,39] and highly concentrated electrolytes[40,41] have been employed to create an effective SEI. Notably, a LiF-rich SEI has been reported that can significantly strengthen the electrode/electrolyte interfaces,[34−36] and as an electrical insulator (10^{-31} S cm^{-1}), LiF can inhibit the accumulation of dead Li.[34] Zhang et al.[35] and Thenuwara et al.[36] have shown the enhanced utilization of Li regulated by the FEC-induced LiF-rich SEI in liquid electrolytes. Therefore, the adopted in situ generated GPEs with in-built fluorinated solid electrolyte interface are expected to be a feasible strategy for safer LMBs with improved performance.

In this work, we propose the in situ conversion of cyclic 1,3-dioxolane (DOL)-based electrolyte into GPE via $LiPF_6$-initiated ring-opening polymerization and the simultaneous creation of a LiF-rich SEI by addition of FEC. The GPE@FEC with high bulk and interfacial ionic conductivity enables a steady Li plating/stripping behavior with low voltage hysteresis. The unique quasi-solid electrolyte displays a high oxidative stability beyond 5.0 V. In addition, a fast interfacial charge transport across the SEI at low temperature has been shown. As a demonstration, symmetric Li||Li cells with GPE@FEC are capable of cycling for 400 h, along with a low voltage hysteresis of ca. 30 mV at 0.5 mA cm^{-2}. When they are matched with a commercial $LiFePO_4$ (LFP) cathode, the Li||LFP cells deliver a steady capacity exceeding 100 mAh g^{-1} for 1000 cycles at 2 C (1 C = 170 mA g^{-1}).

2. EXPERIMENTAL SECTION

2.1. Preparation of Electrolytes. The in situ gel polymer electrolyte of GPE@FEC was obtained with the addition of 2 M lithium hexafluorophosphate ($LiPF_6$, ≥99%, Innochem) and 10% fluoroethylene carbonate (FEC, ≥99%, Adamas) additive (by volume) into the ether-based liquid electrolyte (LE) in a glovebox filled with Ar. The LE was prepared by dissolving 1 M lithium bis(trifluoromethanesulfonyl)imide (LiTFSI) and 0.2 M lithium nitrate ($LiNO_3$) into 1,2-dimethoxyethane/1,3-dioxolane (DME/

https://doi.org/10.1021/acsami.1c19663
ACS Appl. Mater. Interfaces 2021, 13, 60054−60062

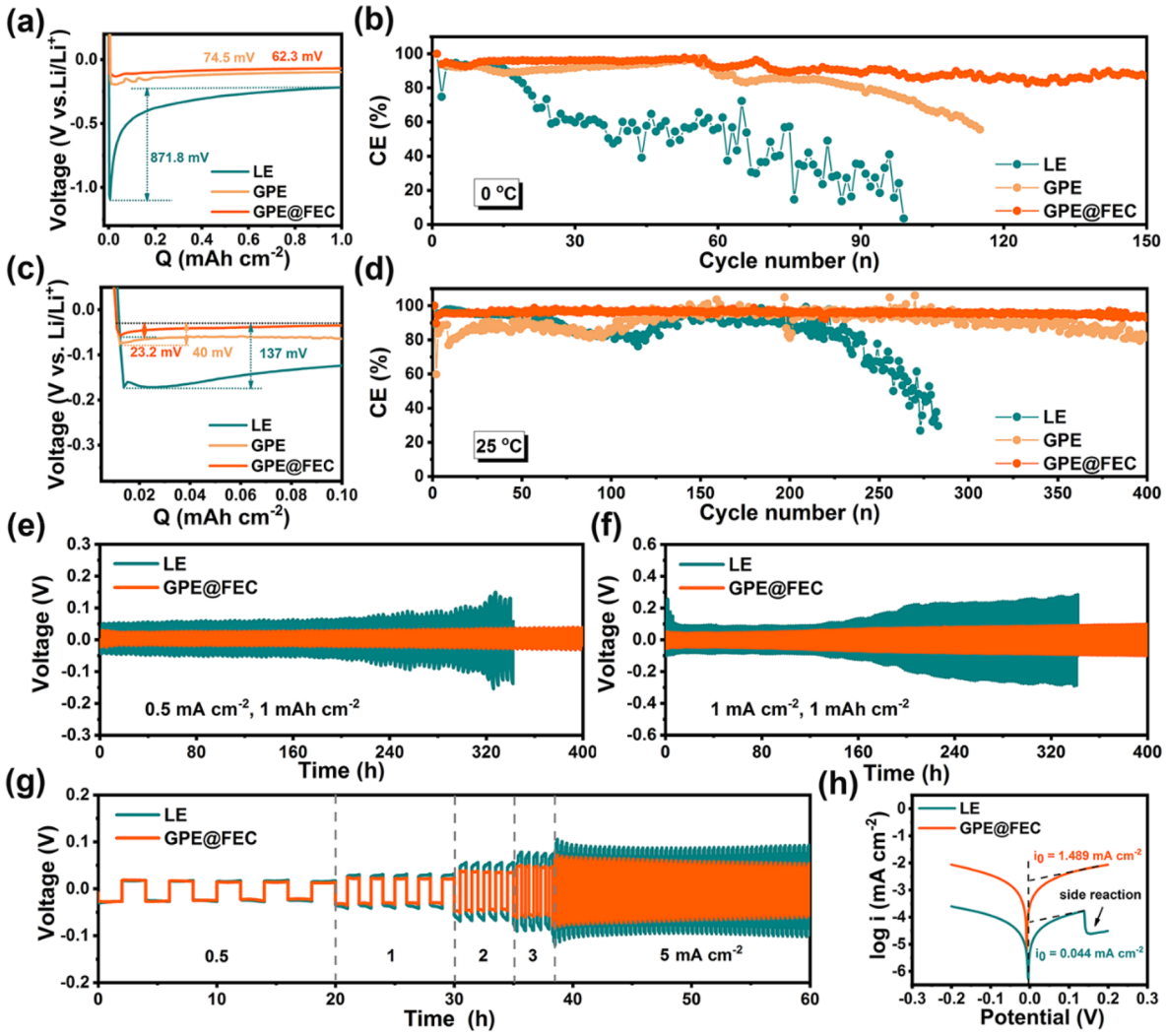

Figure 2. Electrochemical characterizations of Li||Cu and Li||Li cells with different electrolytes. Voltage profiles of nucleation overpotential and Coulombic efficiency of Li||Cu cells at (a, b) 0 °C and (c, d) 25 °C. The current density is 0.5 mA cm^{-2} with a fixed capacity of 1 mAh cm^{-2}. (e, f) Voltage profiles of symmetric Li||Li cells at 0.5 mA cm^{-2} for 1 mAh cm^{-2} and at 1 mA cm^{-2} for 1 mAh cm^{-2}. (g) Voltage profiles of Li||Li cells at different current densities. (h) Tafel curves of Li||Li cells in the range of −0.2 to 0.2 V at a sweep rate of 5 mV s^{-1}.

DOL, 1:1 by volume). The in situ GPE without adding FEC was tested as well for the systemic study. The precursor solution of electrolytes was spontaneously transformed into GPE and GPE@FEC after standing for ca. 12 h at room temperature.

2.2. Material Characterizations. The material characterizations were conducted at ambient temperature. The nuclear magnetic resonance (NMR) was performed on a Varian 600 MHz spectrometer. The Fourier transform infrared (FTIR) spectra were detected in the range of 400−4000 cm^{-1} by thermo Nicolet iS50. For the measurement of gel-permeation chromatography (GPC, Agilent 1260), the GPE@FEC was dissolved in tetrahydrofuran and sonicated to a concentration of approximately 1 mg mL^{-1}. Scanning electron microscopy (SEM) was performed on JSM-7500F and combined with energy-dispersive X-ray spectroscopy (EDS). X-ray photoelectron spectroscopy (XPS) was conducted on a spectrometer (Escalab 250Xi) with Al Kα X-ray radiation. Contact angles were tested on an optical measuring device (OSA200, Germany). A quartz cell with transparent quartz window (Beijing Scistar Technology Co., Ltd., LIB-MS-II) was assembled with an optical microscope camera (Belona, 200X−800X) for in situ observation of the Li deposition behavior.

2.3. Fabrication of Batteries. The preparation of a $LiFePO_4$-based cathode was as previously reported.[6] In the final dried cathode, the mass ratio of $LiFePO_4$, Ketjen Black, and poly(vinylidene fluoride) was 90:5:5. The aluminum foil (18 μm thick) was used as the current collector. The thickness of the dried electrodes including Al foil is ca. 40 μm, and the loading of LFP is ca. 4 mg cm^{-2}. The Li||LFP coin-type cells were assembled with a metallic-Li anode (d = 14 mm, 0.3 mm thick), which was separated from LFP by a microporous separator (Celgard 2325, d = 18 mm, 25 μm thick). Each cell was injected with 50 μL of electrolyte.

2.4. Electrochemical Tests. The electrochemical tests are performed after storage of the fresh cells for 24 h. The galvanostatic cycling was performed on a battery test system (LAND, Wuhan) at room temperature. The electrochemical impedance spectroscopy (EIS) was tested in the frequency of 0.1−10^6 Hz with an amplitude of 10 mV at the open-circuit potential. Tafel tests of symmetric cells and linear sweep voltammetry (LSV) tests of electrolytes were performed on an electrochemistry workstation (CHI660E, Chenhua) within −0.2−0.2 V or 1−7 V (vs Li/Li$^+$), respectively.

According to the EIS results at temperatures of 0−50 °C, the ionic conductivity (σ) of GPE@FEC is calculated by

$$\sigma = L/RS \quad (1)$$

where L is the thickness of the electrolyte; S is the surface area of the stainless steel; and R is bulk resistance.

According to chronoamperometry and EIS results of Li||Li cells, the lithium transference number (t_{Li+}) of GPE@FEC is calculated by

https://doi.org/10.1021/acsami.1c19663
ACS Appl. Mater. Interfaces 2021, 13, 60054−60062

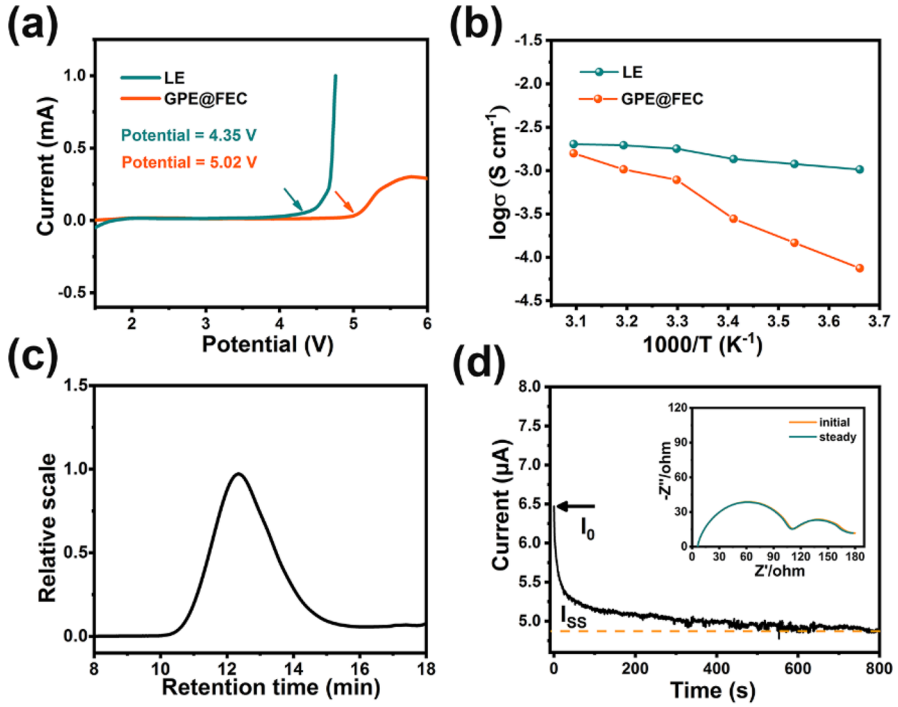

Figure 3. (a) LSV curves of LE and GPE@FEC. (b) The ionic conductivity of LE and GPE@FEC. (c) GPC profile of GPE@FEC; the THF was used as the eluent. (d) The plot of current as a function of time for the symmetric Li||Li cell with GPE@FEC. The inset is the EIS plot of the cell.

$$t_{Li+} = I_{ss}(\Delta V - I_0R_0)/I_0(\Delta V - I_{ss}R_{ss}) \quad (2)$$

where I_0 and I_{SS} are the initial and steady-state currents; ΔV is the polarization potential of 10 mV; and R_0 and R_{SS} are the initial and steady-state resistances.

3. RESULTS AND DISCUSSION

3.1. Synthesis and Characterizations of GPE@FEC. A schematic comparison of the Li anode/electrolyte interphase with ex situ GPE film and $LiPF_6$-initiated in situ formed GPE@FEC is shown in Figure 1a. Briefly, the common ex situ GPE contacts poorly with the Li anode, hindering the interfacial transfer of Li^+ and allowing the uncontrollable dendritic Li growth. In contrast, the GPE@FEC prepared by in situ gelation of liquid electrolyte provided better interfacial contact with the Li anode. With the aid of the film-forming FEC additive, the robust in-bulit LiF-rich SEI layer permits fast interfacial transport of Li ions as well as uniform Li deposition. The contact angle test shows that the precursor solution of GPE@FEC has a contact angle of 16.7° on the $LiFePO_4$ cathode, which is slightly higher than the 16° of LE (Figure S1), indicating the addition of $LiPF_6$ and FEC into LE would not affect the wettability. The gelation of the precursor electrolyte involves a cation-induced ring-opening polymerization of DOL.[21,42] The phosphorus pentafluoride (PF_5) initiator is produced by the spontaneous decomposition of $LiPF_6$, and then PF_5 combines with a trace amount of water to form $H^+(PF_5OH)^-$, which induces the conversion of a DOL monomer to a linear-chain poly-DOL at room temperature. Afterward, a homogeneous GPE@FEC framework can be in situ generated inside the electrochemical cells. The macroscopic optical images show that the precursor solution is transformed into a viscoelastic gel state (Figure 1b), which would reduce the safety risk of flammable liquid electrolyte leakage.

Both NMR and FTIR spectra support the successful polymerization of monomer DOL. The ^1H NMR spectrum of the GPE@FEC-containing dimethyl sulfoxide (DMSO) solution shows the H peaks at 4.69 and 3.66 ppm (Figure 1c), belonging to H atoms of poly-DOL, whereas the ^1H NMR of monomer DOL shows the absence of the two characteristic H peaks, indicating the DOL has been polymerized into poly-DOL in GPE@FEC (Figure S2). The ^{13}C NMR spectrum confirms that the chemical shift at 64.23 ppm corresponds to the C group of $-O-CH_2-CH_2-O-$ and at 94.67 ppm corresponding to $-O-CH_2-O-$ (Figure 1d).[21,43] To estimate the degree of polymerization, we integrated the ^1H peak areas of the redundant DOL and the poly-DOL. As summarized in Table S1, the polymerization degree of DOL is 87.6%. The FTIR spectra reveal the structural difference between the quasi-solid and liquid electrolytes (Figure 1e). After gelation, the clear change in the position of the $-O-C-$ vibration, the disappearance of the C−H out-of-plane vibration, and the appearance of the long-chain $-C-C-$ vibration at 840 cm^{-1} indicate the polymerization of DOL.[44] In addition, the chemical structure of the polymer framework remains stable over time, as verified by the FTIR spectra of the electrolyte after gelation for 1, 2, and 7 days (Figure S3).

3.2. Electrochemical Characteristics of GPE@FEC. The effect of FEC additive on the SEI properties was evaluated first by the Li plating/stripping with Li||Cu cells at different temperatures. Under 0 °C, a sharp voltage drop (871.8 mV) during the initial Li nucleation stage is observed with LE (Figure 2a) at 0.5 mA cm^{-2}, which is much higher than that with in situ formed GPE (74.5 mV) or GPE@FEC (62.3 mV). The Li||Cu cell using LE delivers very low Coulombic efficiency (CE) ranging from 60% to 0% after 20 cycles with a capacity of 1 mAh cm^{-2} (Figure 2b). With GPE, a high CE above 90% can be maintained for some time; however, it decays quickly after 50 cycles. The CE of the cell with GPE@

https://doi.org/10.1021/acsami.1c19663
ACS Appl. Mater. Interfaces 2021, 13, 60054−60062

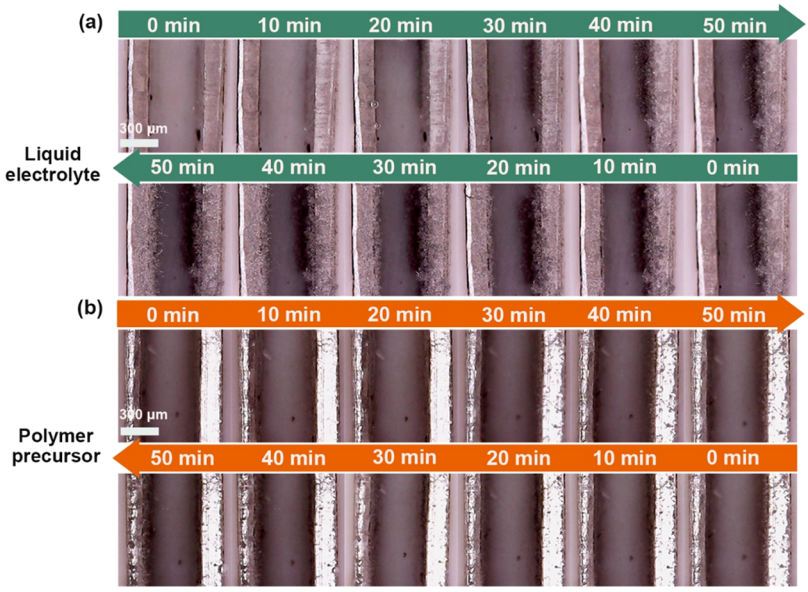

Figure 4. In situ optical microscopy observations on the electrode/electrolyte interface of the symmetric Li||Li cells with (a) LE and (b) the precursor solution of GPE@FEC during Li plating/stripping at a current density of 0.5 mA cm^{-2}.

FEC keeps stable at ~90% after 100 cycles, reflecting the significant role of FEC on regulation of Li deposition behavior at low temperature. At 25 °C, an initial nucleation phase of 137 mV is shown for the Li||Cu cell with LE, which decreases to 23.2 mV with GPE@FEC (Figure 2c). The plating/stripping profiles show the steady-state cycling with GPE@FEC (Figure S4). The GPE@FEC exhibits a higher CE > 98.7% over 400 cycles, compared to that of 60% less than 250 cycles with LE (Figure 2d). The microstructure of Li deposits on Cu at various temperatures was studied by optical and SEM images (Figure S5). The deposited Li exhibits a loose and dendritic morphology with LE, irrespective of at 0 or 25 °C. Notably, the surface of deposited Li with GPE@FEC shows much a denser surface with larger Li particle size, contributing to alleviating side interfacial reactions.

The Li deposition behavior was also investigated with the symmetric Li||Li cells. At 0.5 mA cm^{-2} for 1 mAh cm^{-2}, the overpotential of the cell with LE increases to 150 mV after cycling of 320 h, whereas that with GPE@FEC is performed at a significantly lower ca. 30 mV (Figure 2e). The voltage hysteresis remains below 50 mV after 400 h. At 1 mA cm^{-2}, the Li||Li cell with LE suffers from a large polarization of 200 mV upon the 200 h (Figure 2f). In contrast, the steady cycling of the cell using GPE@FEC can be maintained at a low overpotential for more than 400 h. The value of voltage hysteresis functions with cyclic time supplies a clearer estimation of the stable Li deposition/dissolution behavior with GPE@FEC (Figure S6). Even at 2 mA cm^{-2}, the Li||Li cell can cycle stably for 200 h without exceeding a voltage hysteresis of 130 mV (Figure S7), and increasing to 5 mA cm^{-2}, the cell with GPE@FEC also shows lower voltage polarization compared to LE (Figure 2g). The exchange current density of GPE@FEC/Li (I_o = 1.489 mA cm^{-2}) is much larger than that of LE/Li (I_o = 0.044 mA cm^{-2}) (Figure 2h), suggesting a faster interfacial transport of Li ions.

The oxidative stability of the electrolytes was estimated by the electrochemical window. The LSV curve of GPE@FEC shows a higher electrochemical window under 5.02 V than that of 4.35 V for LE (Figure 3a). The in situ constructed GPE@FEC demonstrates a bulk ionic conductivity of 7.81 × 10^{-4} S cm^{-1} at ambient temperature (Figure 3b). The value can be ranked in the high level in comparison with the other GPEs (Table S2). The GPC measurement (Figure 3c and Table S3) shows that the number-average molecular weight (M_n) and molecular weight (M_w) of the GPE@FEC is as high as 4.6 × 10^4 and 9.0 × 10^4, respectively. The value of polydispersity (PDI) is 1.95, which is lower than published reports,[23,45] indicating the formation of poly-DOL chains with uniform length. Besides, GPE@FEC exhibits a good Li transference number (t_{Li+}) of 0.71 (Figure 3d), reflecting the good mobility of Li ions.

3.3. Electrochemical Lithium Plating/Stripping Mechanism. In situ optical microscopy, as the illustration shows in Figure S8, has been applied as an effective technique to observe Li dendrites.[46,47] The precursor solution of GPE@FEC and LE was injected into the symmetric Li||Li cells, respectively. The smooth surface of fresh Li can be seen before a Li plating/stripping test at 0 min. After plating for 30 min at 0.5 mA cm^{-2}, mossy Li dendrites are visible on the Li electrode with LE (Figure 4a). Increasing the plating time to 50 min, the dendrites grow more thick and start to accumulate at localized areas. During the reverse stripping, the mossy Li dendrites are also observed on the counter Li electrode. When using the precursor solution of GPE@FEC, the mossy and dendric Li deposition is greatly suppressed (Figure 4b), indicating a robust SEI has been constructed before the transformation of a gel state electrolyte.

The microscopic view of the Li surface after cycling for 100 h at 0.5 mA cm^{-2}, and 1 mAh cm^{-2} was further investigated by SEM. The pristine Li foil shows a smooth surface and a thickness of 301 μm (Figure 5a). The predominantly mossy dendritic Li surface is shown after cycling in LE (Figure 5b). The loosely packed Li deposition leads to the severe expansion of Li foil to ca. 397 μm. Meanwhile, optical and SEM images of the separator confirm the adsorbent dark broken Li dendrites (Figure S9a). In comparison, the Li metal that uses GPE@FEC shows the dense deposition of Li (Figure 5c), showing an expansion of less than 2% in thickness, and the separator is

https://doi.org/10.1021/acsami.1c19663
ACS Appl. Mater. Interfaces 2021, 13, 60054−60062

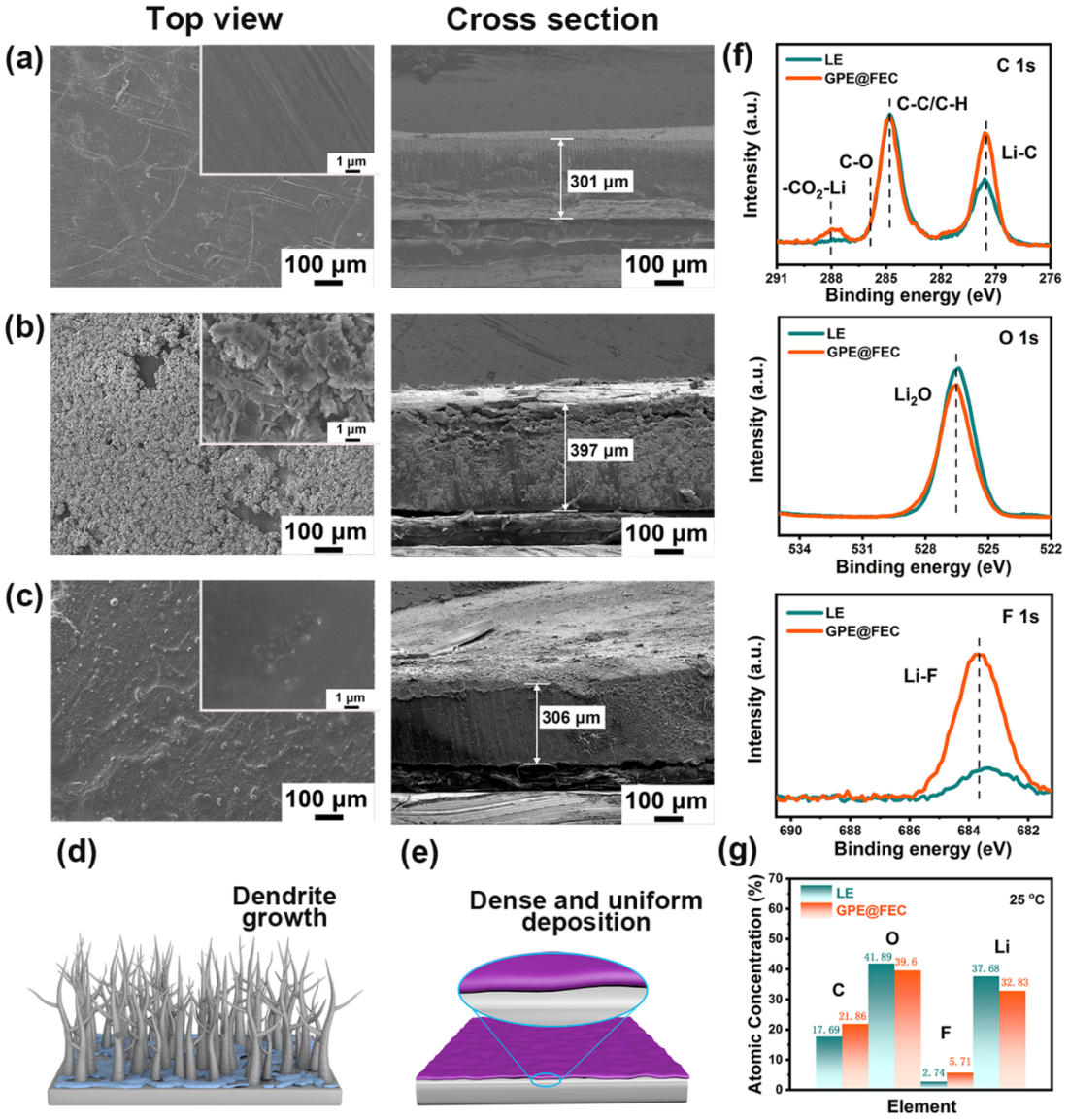

Figure 5. Top-view and cross-sectional SEM images of (a) pristine Li and Li deposition morphology in Li||Li cells with (b) LE and (c) GPE@FEC, respectively. The inset of (a), (b), and (c) are high-magnification images. Schematic surface morphology of Li after plating in (d) LE and (e) GPE@FEC. (f) High-resolution C 1s, O 1s, and F 1s XPS spectra of the Li−metal surface with LE or GPE@FEC. (g) Atomic ratios of elements in the surface of Li.

clean and free of dark Li dendrites (Figure S9b). The surface evolution of the Li electrodes with LE and GPE@FEC can be depicted schematically. During cycling, the side reactions between LE and Li cause erosion and random deposition of Li (Figure 5d). Instead, the robust SEI of the Li with GPE@FEC ensures a high Li plating/stripping efficiency (Figure 5e). The microscopic view supports the critical role of FEC on the formation of the SEI, which presents a strong ability for the stabilization of the Li/electrolyte interface.

The uniform distribution of C, O, F, and sparse P in the SEI with GPE@FEC was observed from the EDS images (Figure S10). The chemical composition of the SEI with LE or GPE@FEC was probed by XPS. The survey XPS spectra show the same peak positions of C, O, F, and Li for the SEI with LE and GPE@FEC (Figure S11).[36] As shown in Figure 5f, three peaks including $-CO_3-Li$, C−C/C−H, and Li−C are shown at 287.9, 284.8, and 279.6 eV, respectively, in the C 1s spectra. Nevertheless there is a prominent increase of the intensity in terms of the $-CO_3-Li$ and Li−C peaks with GPE@FEC, suggesting an increase of Li-ion conducive inorganic species.[42] The O 1s spectra reveal that the Li_2O is formed with both electrolytes. The F 1s spectrum of the SEI with GPE@FEC shows an obviously higher intensity of the peak at 683.4 eV, which is the characteristic peak of LiF. According to the area of the LiF peak, the surface F content increases from 2.74% for LE to 5.71% for GPE@FEC (Figure 5g), which is ascribed to the reduction of FEC on the Li surface. The compact SEI with high inorganic components would facilitate the charge transfer as well as prevent the continuous decomposition of electrolyte.

3.4. Cell Performance with $LiFePO_4$ Cathode. To evaluate the feasibility of the GPE@FEC electrolyte in the practical batteries with commercial cathodes, the LFP cathode was adopted to assemble Li||LFP cells. The cycling of the cells using LE or GPE@FEC at a current rate of 0.5 C (1 C = 170 mA g^{-1}) is shown in Figure 6a. The cells deliver almost the same specific capacity at initial cycles. However, gradual

https://doi.org/10.1021/acsami.1c19663
ACS Appl. Mater. Interfaces 2021, 13, 60054−60062

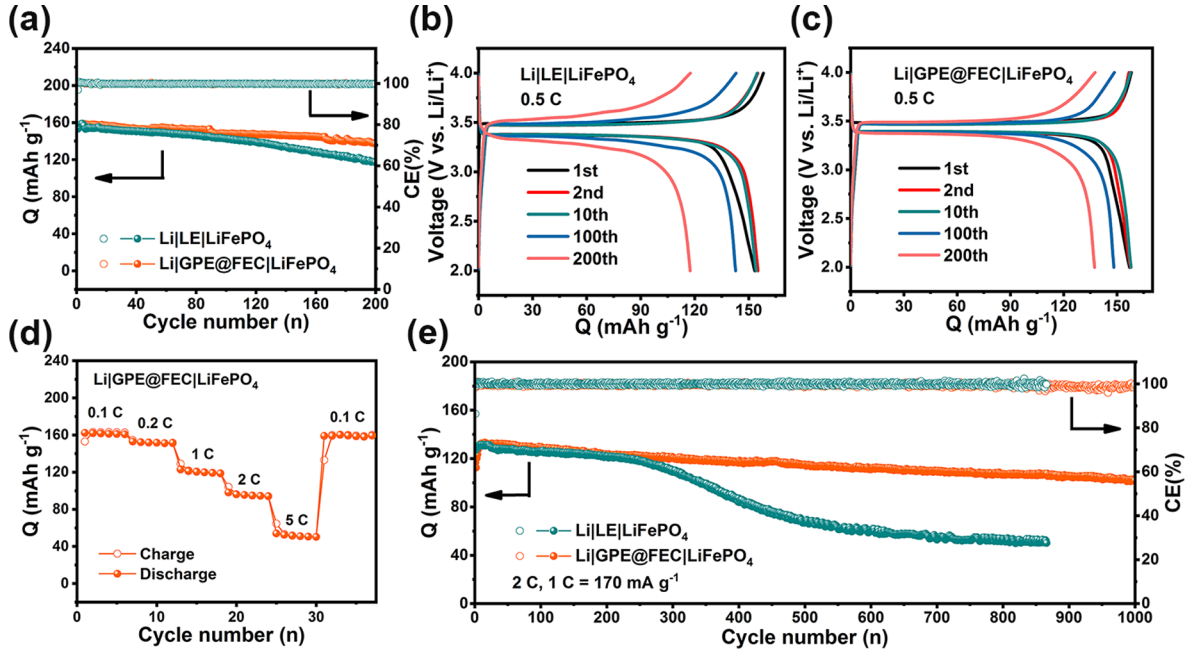

Figure 6. Electrochemical tests of the Li||$LiFePO_4$ cells with LE and GPE@FEC. (a) Cycling performance and the corresponding voltage−capacity curves with (b) LE and (c) GPE@FEC at a current rate of 0.5 C (1 C = 170 mA g^{-1}). (d) Rate performance measured at different current densities. (e) Cycling performance at 2 C.

capacity fading is observed for the cell with LE after 100 cycles, along with increased voltage polarization between charge and discharge profiles (Figure 6b). In contrast, the cell with GPE@FEC shows improved cycling with lower polarization (Figure 6c). The rate capability test shows that the reversible capacity could recover to 160 mAh g^{-1} from 5 to 0.1 C quickly, indicating a good reversibility (Figure 6d). The long-term cycling at 2 C shows a significant capacity decay of 47.2% over 500 cycles for the cell with LE (Figure 6e). Instead, the cell delivers 102 mAh g^{-1} over 1000 cycles with a capacity retention rate of 77.6%. The SEM image reveals the rough Li-anode surface with inhomogeneous deposits for cells with LE after long-term cycling (Figure S12a). The compact and homogeneous Li surface (Figure S12b) of the cell with GPE@FEC further prove its dendrite inhibition effects.

4. CONCLUSIONS

In summary, we demonstrate the in situ construction of the GPE along with the in-built fluorinated SEI for dendrite-free Li−metal batteries. By encapsulating the liquid electrolyte and FEC additive into the matrix of poly-DOL, a quasi-solid electrolyte and a LiF-rich SEI are obtained simultaneously. Therefore, the thermal runaway due to the leakage of liquid inflammable solvents and uncontrollable Li dendrites are greatly suppressed. The robust fluorinated SEI functions as a Li^+ conductor and prevents sustained electrolyte decomposition during the prolonged cycles. In addition, it guides the uniform deposition of Li by regulating the Li^+ flux. The high bulk and interfacial transference of Li^+ guarantee the stable LMBs. The symmetric Li||Li cells with the GPE@FEC exhibit improved cycling stability and rate capability, especially at low temperature. The cells with a commercial cathode further demonstrate the feasibility of the rationally designed GPE@FEC, providing an alternative solution for safe and high-energy Li-metal batteries.

■ ASSOCIATED CONTENT

Supporting Information

The Supporting Information is available free of charge at https://pubs.acs.org/doi/10.1021/acsami.1c19663.

Contact angle measurements of electrolytes; polymerization degree of DOL; the galvanostatic charge/discharge profiles of Li||Cu cells with LE, GPE, and GPE@FEC; optical photographs and SEM images of Cu foil after Li deposition in LE and GPE@FEC at different temperatures; voltage hysteresis of Li||Li cells with LE and GPE@FEC; M_n, M_w, and PDI values for GPE@FEC, obtained via GPC; illustration of in situ optical microscopy; surface morphology of separators with LE and GPE@FEC after cycling; elemental mapping images Li surface; and the survey XPS spectra of the cycled Li surface (PDF)

■ AUTHOR INFORMATION

Corresponding Authors

Lina Wang − *State Key Laboratory for Modification of Chemical Fibers and Polymer Materials, College of Materials Science and Engineering, Donghua University, Shanghai 201620, China;* orcid.org/0000-0002-2211-4661; Email: linawang@dhu.edu.cn

Yonggang Wang − *Department of Chemistry, Fudan University, Shanghai 200433, China;* orcid.org/0000-0002-2447-4679; Email: ygwang@fudan.edu.cn

Authors

Xiaoxia Jiao − *State Key Laboratory for Modification of Chemical Fibers and Polymer Materials, College of Materials Science and Engineering, Donghua University, Shanghai 201620, China*

Jin Wang − *State Key Laboratory for Modification of Chemical Fibers and Polymer Materials, College of Materials Science*

and Engineering, Donghua University, Shanghai 201620, China

Guixia Gao − *State Key Laboratory for Modification of Chemical Fibers and Polymer Materials, College of Materials Science and Engineering, Donghua University, Shanghai 201620, China*

Xuezhi Zhang − *State Key Laboratory for Modification of Chemical Fibers and Polymer Materials, College of Materials Science and Engineering, Donghua University, Shanghai 201620, China*

Cuimei Fu − *State Key Laboratory for Modification of Chemical Fibers and Polymer Materials, College of Materials Science and Engineering, Donghua University, Shanghai 201620, China*

Tianxi Liu − *State Key Laboratory for Modification of Chemical Fibers and Polymer Materials, College of Materials Science and Engineering, Donghua University, Shanghai 201620, China; Key Laboratory of Synthetic and Biological Colloids, Ministry of Education, School of Chemical and Material Engineering, Jiangnan University, Wuxi 214122, China*

Complete contact information is available at: https://pubs.acs.org/10.1021/acsami.1c19663

Notes

The authors declare no competing financial interest.

■ ACKNOWLEDGMENTS

The authors acknowledge financial support from the National Key Research and Development Program of China (2018YFE0201702), Shanghai Scientific and Technological Innovation Project (18JC1410600), and the National Natural Science Foundation of China (21603030).

■ REFERENCES

(1) Tarascon, J.-M.; Armand, M. Issues and Challenges Facing Rechargeable Lithium Batteries. *Nature* **2001**, *414*, 359−367.

(2) Lin, D.; Liu, Y.; Cui, Y. Reviving the Lithium Metal Anode for High-Energy Batteries. *Nat. Nanotechnol.* **2017**, *12*, 194−206.

(3) Choi, J. W.; Aurbach, D. Promise and Reality of Post-Lithium-Ion Batteries with High Energy Densities. *Nat. Rev. Mater.* **2016**, *1*, 16013.

(4) Li, M.; Lu, J.; Chen, Z.; Amine, K. 30 Years of Lithium-Ion Batteries. *Adv. Mater.* **2018**, *30*, 1800561.

(5) Ju, J.; Ma, J.; Wang, Y.; Cui, Y.; Han, P.; Cui, G. Solid-State Energy Storage Devices Based on Two-Dimensional Nano-Materials. *Energy Storage Mater.* **2019**, *20*, 269−290.

(6) Zhao, C.; Xiong, S.; Li, H.; Li, Z.; Qi, C.; Yang, H.; Wang, L.; Zhao, Y.; Liu, T. A Dendrite-Free Composite Li Metal Anode Enabled by Lithiophilic Co, N Codoped Porous Carbon Nanofibers. *J. Power Sources* **2021**, *483*, 229188.

(7) Liang, Y.; Zhao, C.-Z.; Yuan, H.; Chen, W.; Huang, J.-Q.; Yu, D.; Liu, Y.; Titirici, M.-M.; Chueh, Y.-L.; Yu, H.; Zhang, Q. A Review of Rechargeable Batteries for Portable Electronic Devices. *InfoMater.* **2019**, *1*, 6−32.

(8) Cheng, X.-B.; Zhang, R.; Zhao, C.-Z.; Zhang, Q. Toward Safe Lithium Metal Anode in Rechargeable Batteries: A Review. *Chem. Rev.* **2017**, *117*, 10403−10473.

(9) Zhao, C.; Yao, X.; Yang, H.; Jiao, X.; Wang, L. Hierarchical Porous Carbon Nanofibers with Lithiophilic Metal Oxide Crystalline Grains for Long-Life Li Metal Anodes. *Compos. Commun.* **2021**, *26*, 100789.

(10) Fu, K.; Gong, Y.; Liu, B.; Zhu, Y.; Xu, S.; Yao, Y.; Luo, W.; Wang, C.; Lacey, S. D.; Dai, J.; Chen, Y.; Mo, Y.; Wachsman, E.; Hu, L. Toward Garnet Electrolyte−Based Li Metal Batteries: An Ultrathin, Highly Effective, Artificial Solid-State Electrolyte/Metallic Li Interface. *Sci. Adv.* **2017**, *3*, No. e1601659.

(11) Gao, Z.; Sun, H.; Fu, L.; Ye, F.; Zhang, Y.; Luo, W.; Huang, Y. Promises, Challenges, and Recent Progress of Inorganic Solid-State Electrolytes for All-Solid-State Lithium Batteries. *Adv. Mater.* **2018**, *30*, 1705702.

(12) Fan, L.; Wei, S.; Li, S.; Li, Q.; Lu, Y. Recent Progress of the Solid-State Electrolytes for High-Energy Metal-Based Batteries. *Adv. Energy Mater.* **2018**, *8*, 1702657.

(13) Jena, A.; Meesala, Y.; Hu, S.-F.; Chang, H.; Liu, R.-S. Ameliorating Interfacial Ionic Transportation in All-Solid-State Li-Ion Batteries with Interlayer Modifications. *ACS Energy Lett.* **2018**, *3*, 2775−2795.

(14) Manthiram, A.; Yu, X.; Wang, S. Lithium Battery Chemistries Enabled by Solid-State Electrolytes. *Nat. Rev. Mater.* **2017**, *2*, 16103.

(15) Yan, C.; Zhu, P.; Jia, H.; Zhu, J.; Selvan, R. K.; Li, Y.; Dong, X.; Du, Z.; Augunawela, I.; Wu, N.; Dirican, M.; Zhang, X. High-Performance 3-D Fiber Network Composite Electrolyte Enabled with Li-Ion Conducting Nanofbers and Amorphous PEO-Based Cross-Linked Polymer for Ambient All-Solid-State Lithium-Metal Batteries. *Adv. Fiber Mater.* **2019**, *1*, 46−60.

(16) Wang, P.; Chai, J.; Zhang, Z.; Zhang, H.; Ma, Y.; Xu, G.; Du, H.; Liu, T.; Li, G.; Cui, G. An Intricately Designed Poly(Vinylene Carbonate-Acrylonitrile) Copolymer Electrolyte Enables 5 V Lithium Batteries. *J. Mater. Chem. A* **2019**, *7*, 5295−5304.

(17) Feng, L.; Wang, K.; Zhang, X.; Sun, X.; Li, C.; Ge, X.; Ma, Y. Flexible Solid-State Supercapacitors with Enhanced Performance from Hierarchically Graphene Nanocomposite Electrodes and Ionic Liquid Incorporated Gel Polymer Electrolyte. *Adv. Funct. Mater.* **2018**, *28*, 1704463.

(18) Zhao, D.; Martinelli, A.; Willfahrt, A.; Fischer, T.; Bernin, D.; Khan, Z. U.; Shahi, M.; Brill, J.; Jonsson, M. P.; Fabiano, S.; Crispin, X. Polymer Gels with Tunable Ionic Seebeck Coefficient for Ultra-Sensitive Printed Thermopiles. *Nat. Commun.* **2019**, *10*, 1093.

(19) Bachman, J. C.; Muy, S.; Grimaud, A.; Chang, H.-H.; Pour, N.; Lux, S. F.; Paschos, O.; Maglia, F.; Lupart, S.; Lamp, P.; Giordano, L.; Yang, S.-H. Inorganic Solid-State Electrolytes for Lithium Batteries: Mechanisms and Properties Governing Ion Conduction. *Chem. Rev.* **2016**, *116*, 140−162.

(20) Zhang, X.; Liu, T.; Zhang, S.; Huang, X.; Xu, B.; Liu, Y.; Xu, B.; Li, L.; Nan, C.-W.; Shen, Y. Synergistic Coupling between $Li_{6.75}La_3Zr_{1.75}Ta_{0.25}O_{12}$ and Poly(vinylidene fluoride) Induces High Ionic Conductivity, Mechanical Strength, and Thermal Stability of Solid Composite Electrolytes. *J. Am. Chem. Soc.* **2017**, *139*, 13779−13785.

(21) Liu, F.-Q.; Wang, W.-P.; Yin, Y.-X.; Zhang, S.-F.; Shi, J.-L.; Wang, L.; Zhang, X.-D.; Zheng, Y.; Zhou, J.-J.; Li, L.; Guo, Y.-G. Upgrading Traditional Liquid Electrolyte Via In Situ Gelation for Future Lithium Metal Batteries. *Sci. Adv.* **2018**, *4*, No. eaat5383.

(22) Zuo, T.-T.; Shi, Y.; Wu, X.-W.; Wang, P.-F.; Wang, S.-H.; Yin, Y.-X.; Wang, W.-P.; Ma, Q.; Zeng, X.-X.; Ye, H.; Wen, R.; Guo, Y.-G. Constructing a Stable Lithium Metal-Gel Electrolyte Interface for Quasi-Solid-State Lithium Batteries. *ACS Appl. Mater. Interfaces* **2018**, *10*, 30065−30070.

(23) Wang, C.; Zhang, H.; Dong, S.; Hu, Z.; Hu, R.; Wang, T.; Cui, G.; Chen, L. High Polymerization Conversion and Stable High-Voltage Chemistry Underpinning an In Situ Formed Solid Electrolyte. *Chem. Mater.* **2020**, *32*, 9167−9175.

(24) Tan, S.-J.; Yue, J.; Tian, Y.-F.; Ma, Q.; Wan, J.; Xiao, Y.; Zhang, J.; Yin, Y.-X.; Wen, R.; Xin, S.; Guo, Y.-G. In-Situ Encapsulating Flame-Retardant Phosphate into Robust Polymer Matrix for Safe and Stable Quasi-Solid-State Lithium Metal Batteries. *Energy Storage Mater.* **2021**, *39*, 186−193.

(25) Duan, H.; Yin, Y.-X.; Zeng, X.-X.; Li, J.-Y.; Shi, J.-L.; Shi, Y.; Wen, R.; Guo, Y.-G.; Wan, L.-J. In-Situ Plasticized Polymer Electrolyte with Double-Network for Flexible Solid-State Lithium-Metal Batteries. *Energy Storage Mater.* **2018**, *10*, 85−91.

(26) Huang, S.; Cui, Z.; Qiao, L.; Xu, G.; Zhang, J.; Tang, K.; Liu, X.; Wang, Q.; Zhou, X.; Zhang, B.; Cui, G. An In-Situ Polymerized

Solid Polymer Electrolyte Enables Excellent Interfacial Compatibility In Lithium Batteries. *Electrochim. Acta* **2019**, *299*, 820−827.
(27) Ma, Q.; Zeng, X.-X.; Yue, J.; Yin, Y.-X.; Zuo, T.-T.; Liang, J.-Y.; Deng, Q.; Wu, X.-W.; Guo, Y.-G. Viscoelastic and Nonflammable Interface Design−Enabled Dendrite-Free and Safe Solid Lithium Metal Batteries. *Adv. Energy Mater.* **2019**, *9*, 1803854.
(28) Xu, D.; Su, J.; Jin, J.; Sun, C.; Ruan, Y.; Chen, C.; Wen, Z. In Situ Generated Fireproof Gel Polymer Electrolyte with $Li_{6.4}Ga_{0.2}La_3Zr_2O_{12}$ As Initiator and Ion-Conductive Filler. *Adv. Energy Mater.* **2019**, *9*, 1900611.
(29) Chen, J.; Yang, Z.; Liu, G.; Li, C.; Yi, J.; Fan, M.; Tan, H.; Lu, Z.; Yang, C. Reinforcing Concentrated Phosphate Electrolytes with In-Situ Polymerized Skeletons for Robust Quasi-Solid Lithium Metal Batteries. *Energy Storage Mater.* **2020**, *25*, 305−312.
(30) Ke, X.; Wang, Y.; Dai, L.; Yuan, C. Cell Failures of All-Solid-State Lithium Metal Batteries with Inorganic Solid Electrolytes: Lithium Dendrites. *Energy Storage Mater.* **2020**, *33*, 309−328.
(31) Zhao, Y.; Bai, Y.; Li, W.; An, M.; Bai, Y.; Chen, G. Design Strategies for Polymer Electrolytes with Ether and Carbonate Groups for Solid-State Lithium Metal Batteries. *Chem. Mater.* **2020**, *32*, 6811−6830.
(32) Bae, J.; Zhang, X.; Guo, X.; Yu, G. A General Strategy of Anion-Rich High-Concentration Polymeric Interlayer for High-Voltage, All-Solid-State Batteries. *Nano Lett.* **2021**, *21*, 1184−1191.
(33) Yao, Y.-X.; Zhang, X.-Q.; Li, B.-Q.; Yan, C.; Chen, P.-Y.; Huang, J.-Q.; Zhang, Q. A Compact Inorganic Layer for Robust Anode Protection in Lithium-Sulfur Batteries. *InfoMater.* **2020**, *2*, 379−388.
(34) Liu, Q.-C.; Xu, J.-J.; Yuan, S.; Chang, Z.-W.; Xu, D.; Yin, Y.-B.; Li, L.; Zhong, H.-X.; Jiang, Y.-S.; Yan, J.-M.; Zhang, X.-B. Artificial Protection Film on Lithium Metal Anode toward Long-Cycle-Life Lithium−Oxygen Batteries. *Adv. Mater.* **2015**, *27*, 5241−5247.
(35) Zhang, X.-Q.; Cheng, X.-B.; Chen, X.; Yan, C.; Zhang, Q. Fluoroethylene Carbonate Additives to Render Uniform Li Deposits in Lithium Metal Batteries. *Adv. Funct. Mater.* **2017**, *27*, 1605989.
(36) Thenuwara, A. C.; Shetty, P. P.; Kondekar, N.; Sandoval, S. E.; Cavallaro, K.; May, R.; Yang, C.-T.; Marbella, L. E.; Qi, Y.; McDowell, M. T. Efficient Low-Temperature Cycling of Lithium Metal Anodes by Tailoring the Solid Electrolyte Interphase. *ACS Energy Lette.* **2020**, *5*, 2411−2420.
(37) Ota, H.; Shima, K.; Ue, M.; Yamaki, J.-i. Effect of Vinylene Carbonate as Additive to Electrolyte for Lithium Metal Anode. *Electrochim. Acta* **2004**, *49*, 565.
(38) Lu, Y.; Tu, Z.; Shu, J.; Archer, L. A. Stable Lithium Electrodeposition in Salt-Reinforced Electrolytes. *J. Power Sources* **2015**, *279*, 413−418.
(39) Lu, Y.; Tu, Z.; Archer, L. A. Stable Lithium Electrodeposition in Liquid and Nanoporous Solid Electrolytes. *Nat. Mater.* **2014**, *13*, 961.
(40) Qian, J.; Henderson, W. A.; Xu, W.; Bhattacharya, P.; Engelhard, M.; Borodin, O.; Zhang, J.-G. High Rate and Stable Cycling of Lithium Metal Anode. *Nat. Commun.* **2015**, *6*, 6362.
(41) Suo, L.; Hu, Y.-S.; Li, H.; Armand, M.; Chen, L. A New Class of Solvent-in-Salt Electrolyte for High-Energy Rechargeable Metallic Lithium Batteries. *Nat. Commun.* **2013**, *4*, 1481.
(42) Khan, K.; Tu, Z.; Zhao, Q.; Zhao, C.; Archer, L. A. Synthesis and Properties of Poly-Ether/Ethylene Carbonate Electrolytes with High Oxidative Stability. *Chem. Mater.* **2019**, *31*, 8466−8472.
(43) Siu, S. K-L.; Chung, C. Y-S.; Yam, V. W-W. Amphiphilic Oligo(Ethylene Glycol)- and Poly(Ethyleneoxide)-Block-Poly-(Propylene Oxide)-Block-Poly-(Ethylene Oxide)-Containing Cyclometalated Alkynylgold(III) Complexes: From Basic Photophysics to Self-Assembly and Stimuli-Responsive Properties. *J. Organomet. Chem.* **2017**, *845*, 177−188.
(44) Okada, M.; Yamashita, Y. Y.; Ishii, Y. Polymerization of 1,3-Dioxolane. *Makromol. Chem.* **1964**, *80*, 196−207.
(45) Wang, S.; Zhou, L.; Tufail, M. K.; Yang, L.; Zhai, P.; Chen, R.; Yang, W. In-Situ synthesized Non-Flammable Gel Polymer Electrolyte Enable Highly Safe and Dendrite-Free Lithium Metal Batteries. *Chem. Eng. J.* **2021**, *415*, 128846.
(46) Guo, W.; Han, Q.; Jiao, J.; Wu, W.; Zhu, X.; Chen, Z.; Zhao, Y. In situ Construction of Robust Biphasic Surface Layers on Li Metal for Li-S Batteries with Long Cycle Life. *Angew. Chem., Int. Ed.* **2021**, *60*, 7267−7274.
(47) Wang, H.; He, J.; Liu, J.; Qi, S.; Wu, M.; Wen, J.; Chen, Y.; Feng, Y.; Ma, J. Electrolytes Enriched by Crown Ethers for Lithium Metal Batteries. *Adv. Funct. Mater.* **2021**, *31*, 2002578.

https://doi.org/10.1021/acsami.1c19663
ACS Appl. Mater. Interfaces 2021, 13, 60054−60062